

Manipulating the magnetic properties of $MnBi_2Te_4$ through electrochemical organic molecule intercalation

Yu Du(杜钰), Heng Zhang(张恒), Fuwei Zhou(周福伟), Tianqi Wang(王天奇), Jiajun Li(李佳骏), Wuyi Qi(戚无逸), Yiying Zhang (张祎颖), Yefan Yu(俞业凡), Fucong Fei(费付聪), and Fengqi Song(宋凤麒)
Citation: Chin. Phys. B, 2025, 34 (**8**): 087302. DOI: 10.1088/1674-1056/add5cf
http://cpb.iphy.ac.cn; http://iopscience.iop.org/cpb

What follows is a list of articles you may be interested in

Role of symmetry in antiferromagnetic topological insulators

Sahar Ghasemi and Morad Ebrahimkhas
Chin. Phys. B, 2025, 34 (**7**): 077302. DOI: 10.1088/1674-1056/adcb1e

Higher-order topological corner states and origin in monolayer LaBrO

Qing Wang(王庆) and Ning Hao(郝宁)
Chin. Phys. B, 2024, 33 (**12**): 127303. DOI: 10.1088/1674-1056/ad8a50

Nonvolatile ferroelectric control of electronic properties of Bi_2Te_3

Xusheng Ding(丁旭升), Yunfei Li(李云飞), Chaoyang Kang(康朝阳), Ye-Heng Song(宋业恒), and Weifeng Zhang(张伟风)
Chin. Phys. B, 2024, 33 (**11**): 117301. DOI: 10.1088/1674-1056/ad7670

Negative magnetoresistance in Dirac semimetal Cd_3As_2 with in-plane magnetic field perpendicular to current

Hao-Nan Cui(崔浩楠), Guang-Yu Zhu(祝光宇), Jian-Kun Wang(王建坤), Jia-Jie Yang(杨佳洁), Wen-Zhuang Zheng(郑文壮), Ben-Chuan Lin(林本川), Zhi-Min Liao(廖志敏), Shuo Wang(王硕), and Da-Peng Yu(俞大鹏)
Chin. Phys. B, 2023, 32 (**7**): 077305. DOI: 10.1088/1674-1056/accd50

Correlated insulating phases in the twisted bilayer graphene

Yuan-Da Liao(廖元达), Xiao-Yan Xu(许霄琰), Zi-Yang Meng(孟子杨), and Jian Kang(康健)
Chin. Phys. B, 2021, 30 (**1**): 017305. DOI: 10.1088/1674-1056/abcfa3

RAPID COMMUNICATION

Manipulating the magnetic properties of $MnBi_2Te_4$ through electrochemical organic molecule intercalation

Yu Du(杜钰)[1,4], Heng Zhang(张恒)[1], Fuwei Zhou(周福伟)[1], Tianqi Wang(王天奇)[1], Jiajun Li(李佳骏)[1], Wuyi Qi(戚无逸)[1], Yiying Zhang (张祎颖)[1], Yefan Yu(俞业凡)[1], Fucong Fei(费付聪)[1,†], and Fengqi Song(宋凤麒)[1,2,3,‡]

[1] *National Laboratory of Solid State Microstructures, School of Physics, School of Materials Science and Intelligent Engineering, Collaborative Innovation Center of Advanced Microstructures, Jiangsu Physical Science Research Center, Nanjing University, Nanjing* 210093, *China*

[2] *Atom Manufacturing Institute, Nanjing* 211806, *China*

[3] *Suzhou Laboratory, Suzhou* 215000, *China*

[4] *Suzhou Polytechnic University, Suzhou* 215104, *China*

(Received 7 April 2025; revised manuscript received 1 May 2025; accepted manuscript online 8 May 2025)

$MnBi_2Te_4$, which is emerging as an intrinsic antiferromagnetic (AFM) topological insulator, provides a unique platform to investigate the interplay between magnetism and topology. Modulating its magnetic properties enables the observation of exotic quantum phenomena such as the quantum anomalous Hall effect, axion insulator states, and Majorana fermions. While the intercalation of Bi_2Te_3 can tune its magnetism, synthesizing pure-phase $MnBi_2Te_4$ with uniform Bi_2Te_3 intercalation remains challenging, and the fixed interlayer spacing of Bi_2Te_3 limits magnetic coupling tunability. Here, we utilize electrochemical organic molecule intercalation to expand the van der Waals gap of $MnBi_2Te_4$ and modulate its magnetic properties. Through x-ray diffraction (XRD) characterizations, we confirm that the interlayer spacing of $MnBi_2Te_4$ is expanded from 13.6 Å to 30.5 Å and 61.0 Å by intercalating quaternary ammonium cations (THA^+ and CTA^+), respectively. The THA-$MnBi_2Te_4$ exhibits dual complex magnetic behavior, combining AFM ordering with a Néel temperature (T_N) of 12 K and a small ferromagnetic hysteresis loop at 2 K. The CTA-$MnBi_2Te_4$ shows robust ferromagnetism, with a Curie point (T_C) of 15 K, similar to that of the $MnBi_2Te_4$ monolayer. These results demonstrate that remarkable changes in the magnetic properties of $MnBi_2Te_4$ can be achieved via electrochemical intercalation, providing new insights into manipulating magnetism in layered magnetic materials.

Keywords: topological insulators, electrochemical intercalation, magnetism tuning, van der Waals magnetic materials

PACS: 73.50.–h, 75.70.Cn, 75.50.Pp, 82.45.Aa

DOI: 10.1088/1674-1056/add5cf **CSTR:** 32038.14.CPB.add5cf

1. Introduction

Van der Waals (vdW) layered magnets have garnered significant attention in recent years.[1–6] Owing to their weak interlayer interactions, these materials can be easily exfoliated into ultrathin films and flexibly recombined into diverse heterostructures with novel material properties. Numerous layered magnetic materials have been identified, including $Cr_2Ge_2Te_6$,[7] CrI_3,[8] Fe_3GeTe_2,[9] $FePS_3$,[10] VSe_2,[11] $MnSe_2$,[12] and compounds of the $MnBi_2Te_4$ family,[4,13–30] presenting opportunities for advancements and applications in electronics, spintronics, optoelectronics, and topological physics.[31–33] In particular, intrinsic magnetic topological insulators are promising candidates for achieving a high-temperature quantum anomalous Hall effect (QAHE).[4,13,16–18] $MnBi_2Te_4$, successfully synthesized in recent years, represents a novel intrinsic layered magnetic topological material. $MnBi_2Te_4$ exhibits an A-type antiferromagnetic (AFM) structure with a Néel temperature (T_N) of approximately 25 K, characterized by spins that are aligned ferromagnetically in plane but antiferromagnetically out of plane.[13,16,34] Upon increasing the external field, a spin-flop transition to tilted antiferromagnetism is observed at ±3 T. When the magnetic field reaches ±8 T, the magnetization approaches saturation.[4,17,18] The robust AFM ground state at zero field presents a significant challenge for realizing a QAHE. Notably, it has been predicted that the ferromagnetic (FM) order could persist in a single septuple-layer (SL) block isolated from bulk $MnBi_2Te_4$, suggesting that a $MnBi_2Te_4$ monolayer would be a promising 2D magnetic material. Given that the diverse topological states in $MnBi_2Te_4$ are strongly correlated with the magnetic characteristics of each individual layer, understanding the magnetic behavior of monolayer $MnBi_2Te_4$ becomes crucial. However, mechanically exfoliated monolayers are susceptible to oxidation, making it challenging to measure their magnetic properties. For bulk $MnBi_2Te_4$, a zero-field FM ground state can be real-

†Corresponding author. E-mail: feifucong@nju.edu.cn

‡Corresponding author. E-mail: songfengqi@nju.edu.cn

© 2025 Chinese Physical Society and IOP Publishing Ltd. All rights, including for text and data mining, AI training, and similar technologies, are reserved.

ized if the AFM interactions between the Mn atomic layers are sufficiently suppressed. Upon extending this principle to the Bi_2Te_3intercalated family $MnBi_2Te_4$-$(Bi_2Te_3)_m$ (m = 0, 1, 2, 3),[29,34–49] i.e., $MnBi_4Te_7$, $MnBi_6Te_{10}$, and $MnBi_8Te_{13}$, it becomes apparent that the overall magnetic interaction is weakened by the intercalation of one to three Bi_2Te_3 layers between two adjacent $MnBi_2Te_4$ layers. This would enhance the tunability of the magnetic state and enable corresponding adjustments in the topological structure. Comparative studies have revealed distinct magnetic evolution within the manganese–bismuth–tellurium (MBT) family: $MnBi_4Te_7$ and $MnBi_6Te_{10}$ exhibit weakened antiferromagnetism via Bi_2Te_3 intercalation,[29,35,41,50] with T_N decreasing to around 13 K and 11 K, respectively, yet they retain AFM ground states. While the intercalation of three Bi_2Te_3 layers successfully induces an FM ground state, experimentally synthesizing pure-phase $MnBi_2Te_4$ samples with uniformly intercalated Bi_2Te_3 layers remains challenging, especially for three or more Bi_2Te_3 layers. This fundamentally limits the tunability of magnetic coupling. Moreover, Bi_2Te_3 intercalation is restricted to the generation of fixed interlayer spacing increments, consequently restricting the tunability of both the interlayer spacing and magnetic properties in materials engineering, which poses significant challenges in materials design. Here, we systematically investigate the intercalation of organic molecules into $MnBi_2Te_4$ via an electrochemical process to modulate the interlayer spacing, thereby engineering its magnetic properties. We successfully intercalate tetraheptylammonium cations (THA^+) into the vdW gap of $MnBi_2Te_4$, expanding its interlayer spacing from 13.6 Å to 30.5 Å. In THA-$MnBi_2Te_4$, dual complex magnetic behaviors are observed, in which AFM ordering with T_N = 12 K coexists with FM hysteresis down to 2 K. These results indicate that, although the interlayer AFM interaction has been significantly weakened in THA-$MnBi_2Te_4$ as expected, it still plays a dominant role in its magnetic properties. To further increase the interlayer spacing, we intercalate cetyltrimethylammonium cations (CTA^+) into $MnBi_2Te_4$. The interlayer spacing further expands to 61.0 Å, and the CTA-$MnBi_2Te_4$ sample manifests a long-range FM ground state, with an FM transition temperature (T_C) of 15 K, accompanied by a coercive field (H_C) of 595 Oe. This T_C value closely matches that reported for monolayer $MnBi_2Te_4$ in prior reflective magnetic circular dichroism (RMCD) studies.[51] Our results reveal that molecular intercalation not only expands the interlayer spacing but also fundamentally modifies the interlayer magnetic exchange interactions, thereby driving an AFM-to-FM transition. This strategy establishes a generalized platform for synthesizing materials with tunable magnetism, as supported by structural characterization and mechanistic analysis of interlayer coupling modulation.

2. Results and discussion

2.1. Electrochemical intercalation of organic molecules into bulk $MnBi_2Te_4$

The electrochemical intercalation of organic molecules serves as an effective method for modulating interlayer spacing. Figure 1(a) schematically illustrates the electrochemical molecule intercalation setup used in this study. A layered magnet is anchored to a copper clip using a conductive indium rod. In this system, the graphite rod functions as the anode, whereas the indium-clamped single crystal functions as the cathode. To reduce the influence of electrolytic resistance, we utilize an Ag/AgCl reference electrode. This setup dynamically regulates the applied voltage between the graphite and the sample via a real-time feedback configuration, ensuring a constant potential difference between the sample and the reference electrode throughout the intercalation process. Solutions of the quaternary ammonium salts tetraheptylammonium bromide (THAB) or cetyltrimethylammonium bromide (CTAB) in acetonitrile (20 ml; 5 mg·ml^{-1}) serve as electrolytes. During the intercalation process, a negative voltage of 3.4 V is applied to the $MnBi_2Te_4$ cathode to facilitate the insertion of positively charged cations (THA^+ or CTA^+). The intercalation proceeds for 30 min. Driven by the negative electrochemical potential, THA^+ and CTA^+ cations are intercalated into the vdW gap of $MnBi_2Te_4$, expanding the interlayer spacing and consequently modulating the magnetic properties of $MnBi_2Te_4$. The expanded $MnBi_2Te_4$ crystal is then immediately removed from the electrolytic cell and rinsed with deionized water to remove residual reactants. The $MnBi_2Te_4$ bulk samples investigated in this study are grown by the flux method, exhibiting a layered morphology. The typical dimensions are approximately 3×2 mm^2, and the thickness is around 0.05 mm. As illustrated in Fig. 1(b), $MnBi_2Te_4$ is a layered ternary tetradymite compound with the space group $R\bar{3}m$.[51,52] Its crystal structure comprises a repeating unit of seven atomic layers arranged as Te–Bi–Te–Mn–Te–Bi–Te. These structurally independent units, called SLs, are stacked along the c-axis via vdW forces between adjacent SLs. Below T_N, the spins of Mn^{2+} ions couple ferromagnetically within each SL along the out-of-plane easy axis while exhibit AFM exchange coupling between adjacent SLs, leading to an A-type AFM order. This behavior has been theoretically predicted[22,53] and subsequently confirmed by neutron diffraction experiments.[19] As the interlayer spacing increases, the structure of each SL layer remains unchanged, while the overall magnetic interaction weakens, making the magnetic state more tunable. Consequently, the magnetic ordering of the material evolves from AFM to FM, with the T_C of the $MnBi_2Te_4$ monolayer reaching 15.2 K. Here, the large size of the THA^+ and CTA^+ cations can significantly expand the interlayer spacing of $MnBi_2Te_4$, thereby modulating its magnetic properties.

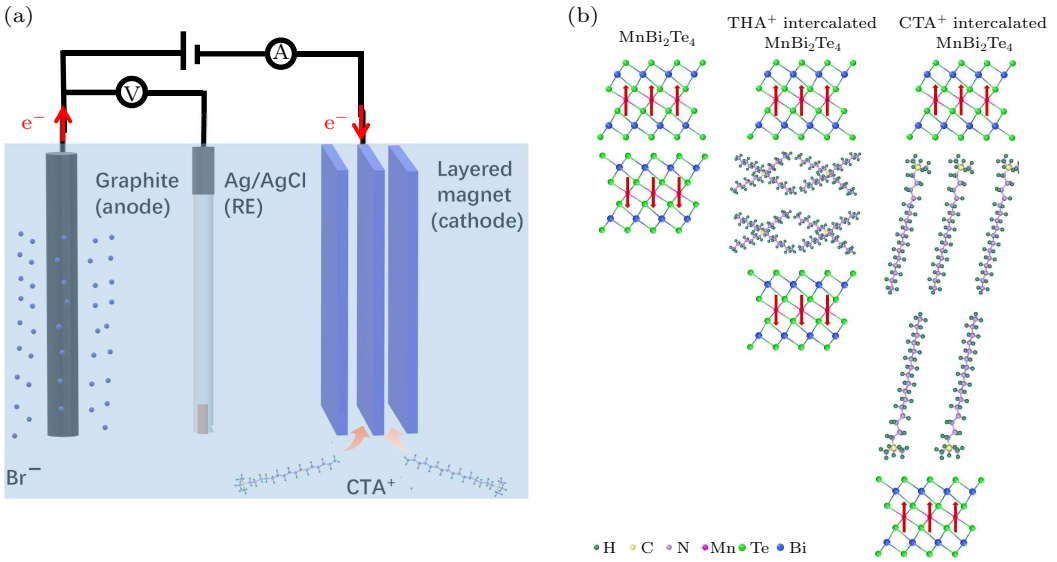


Fig. 1. (a) Schematic diagram of the intercalation apparatus. (b) Schematic illustrations of intercalation with different organic molecules used to control material structures and properties.

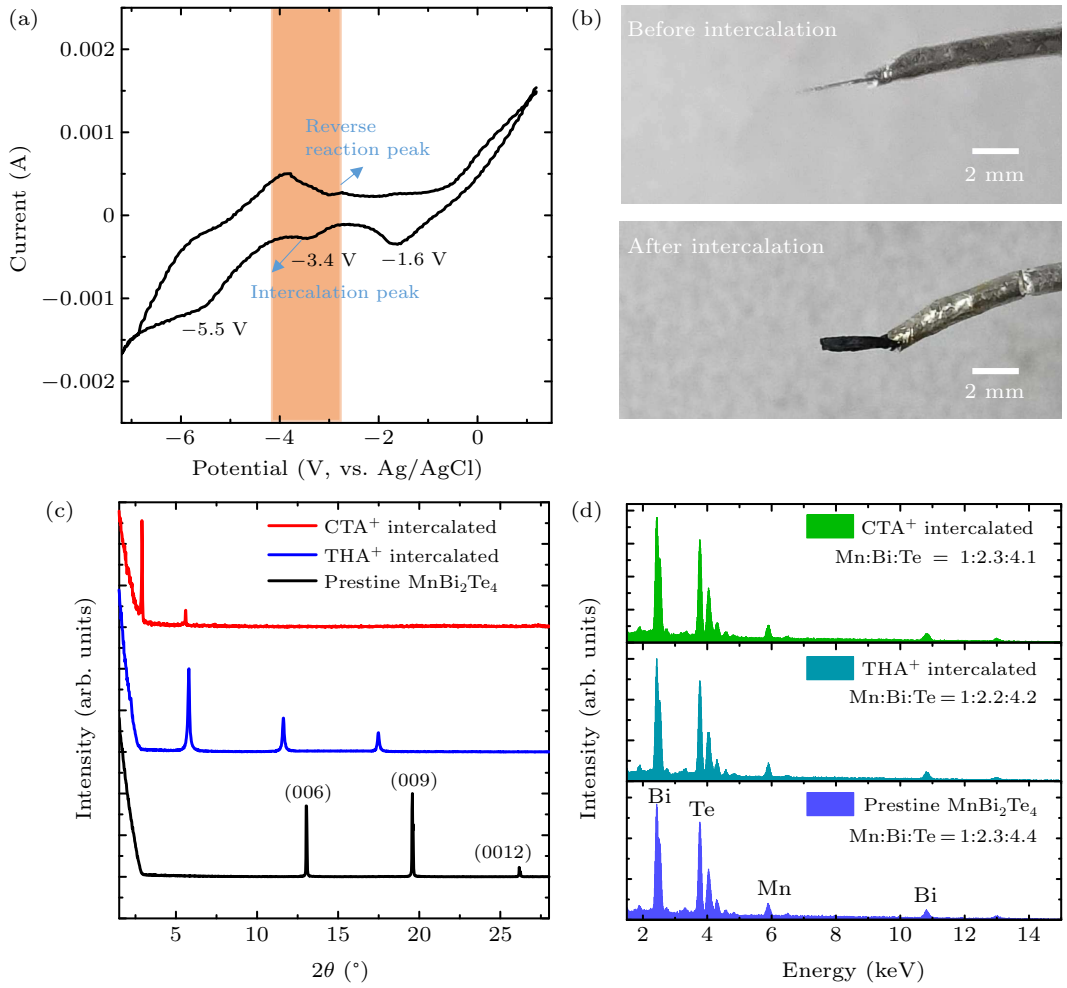


Fig. 2. (a) Cyclic voltammetry curves of CTA-$MnBi_2Te_4$. (b) Optical photographs of the side view of $MnBi_2Te_4$ before and after the intercalation of CTA^+. Scale bar: 2 mm. (c) Direct comparison of XRD results for pristine $MnBi_2Te_4$ (black), THA-$MnBi_2Te_4$ (blue), and CTA-$MnBi_2Te_4$ (red). (d) The EDS data of samples before and after intercalation.

To determine the applied electrochemical potential, we perform cyclic voltammetry (CV) measurements on $MnBi_2Te_4$ in a CTAB–acetonitrile solution, as shown in Fig. 2(a). Three potential peaks are observed at approximately −1.6 V, −3.4 V, and −5.5 V. A reverse reaction peak is also observed at −2.7 V, thereby confirming that the applied electrochemical potential is −3.4 V. When a voltage of −1.6 V is applied, defects in bismuth (Bi) and manganese (Mn) oc-

cur after intercalation, while tellurium (Te) vacancies are observed at −5.5 V. The corresponding energy-dispersive x-ray spectroscopy (EDS) data are provided in Fig. S1 of the supporting information. The upper (lower) panel of Fig. 2(b) displays an optical side-view image of a typical $MnBi_2Te_4$ sample before (after) electrochemical molecule intercalation. Before the electrochemical process, the sample exhibits a metallic luster. Upon completion of the reaction, the structure of the $MnBi_2Te_4$ sample becomes expanded and fluffy. As illustrated in Fig. 2(c), x-ray diffraction (XRD) analysis reveals that the original diffraction peaks of pristine bulk $MnBi_2Te_4$ vanish after the intercalation process, whereas new sets of diffraction peaks corresponding to intercalated $MnBi_2Te_4$ appear. The diffraction peaks corresponding to the $(00n)$ ($n = 6$, 9, 12) planes of pristine bulk $MnBi_2Te_4$ significantly shift to lower diffraction angles in both CTA-$MnBi_2Te_4$ and THA-$MnBi_2Te_4$. This shift reflects a substantial increase in interlayer spacing, from 13.6 Å in pristine bulk $MnBi_2Te_4$ to 30.5 Å in THA-$MnBi_2Te_4$ and 61.0 Å in CTA-$MnBi_2Te_4$. The XRD patterns of the fully intercalated materials exclusively display diffraction peaks corresponding to the expanded lattice, with no detectable signals from the pristine bulk $MnBi_2Te_4$. This indicates both the complete intercalation process and the phase purity of the resulting intercalated superlattices. To verify the elemental composition of $MnBi_2Te_4$ after intercalation, EDS analysis is also performed on both pristine bulk $MnBi_2Te_4$ and samples with intercalated organic cations, as displayed in Fig. 2(d). The results confirm that the atomic ratios of Mn, Bi, and Te remain essentially unchanged.

2.2. Changes in magnetic properties of intercalated $MnBi_2Te_4$

The field-cooled (FC) and zero-field-cooled (ZFC) magnetic susceptibilities of THA-$MnBi_2Te_4$ measured at 0.1 T are shown in Fig. 3(a). The high-temperature paramagnetic behavior culminates in a pronounced peak at 12 K, which is characteristic of AFM ordering. The T_N of only 12 K for the sample, compared to 25 K for pristine $MnBi_2Te_4$, reveals a substantial weakening of the interlayer AFM coupling due to the intercalation of the THA^+ cations between neighboring SLs. Notably, although the AFM interlayer exchange coupling (IEC, which favors AFM states) is weakened, as the spin-flip transition field is significantly lower than that of pure $MnBi_2Te_4$, the IEC still plays an important role in the AFM ground state of THA-$MnBi_2Te_4$. When the temperature further decreases, the AFM-IEC seems not to be the only interaction that influences the magnetic order, as an obvious upturn is observed below T_N for fields applied both in plane and out of plane. The onset of FM interactions, evidenced by the splitting of the FC and ZFC curves at low temperatures, indicates that, despite the overall AFM behavior of THA-$MnBi_2Te_4$, significant FM interactions are present within the material at low temperatures. The $M(H)$ curves of THA-$MnBi_2Te_4$ measured at various temperatures are presented in Fig. 3(b) (out-of-plane field) and Fig. 3(c) (in-plane field). The magnetic field required for magnetization saturation is lower when applied out of plane compared to in plane, suggesting that the easy magnetization axis is oriented along the c-axis. When the temperature is set to 10 K, slightly below T_N, typical AFM $M(H)$ behavior is observed under an out-of-plane magnetic field, with spin–flip upturns appearing at 0.08 T. This magnetic transition field is significantly lower than that of $MnBi_2Te_4$ (3.5 T).[13,19,41] At low temperatures, in the absence of an external field, the magnetization does not drop to zero but instead forms an FM hysteresis loop within the range of −0.01 T to 0.01 T, as observed at $T = 2$ K. However, this kind of FM interaction decays rapidly with increasing thermal energy, leading to the disappearance of magnetic hysteresis above 10 K. These dual complex magnetic behaviors can be attributed to the coexistence of domains with both FM and AFM ordering between neighboring SLs. The field-dependent magnetization along the ab plane exhibits a nonlinear curve below 10 K and displays a small hysteresis at 2 K (Fig. 3(c)). This behavior suggests the presence of an additional magnetic interaction that tends to cant the spins away from their out-of-plane orientation, favoring an FM state.[41] Evidently, the IEC in THA-$MnBi_2Te_4$ is much weaker. To further suppress the IEC, we employ CTA^+ intercalation, which effectively forms a larger interlayer spacing. The magnetic properties of CTA-$MnBi_2Te_4$ are shown in Figs. 3(d)–3(f). As can be seen in Fig. 3(d), the FC and ZFC curves of the CTA-$MnBi_2Te_4$ measured at a field of 0.1 T, both in plane and out of plane, exhibit long-range FM ordering at 15 K, which is comparable to that of the $MnBi_2Te_4$ monolayer (15.2 K) measured by RMCD in previous studies.[51] A pronounced discrepancy between the ZFC and FC data becomes evident as the temperature decreases. The FC and ZFC curves display similar λ-shaped splitting features as displayed in Fig. 3(d), suggesting the formation of FM domains. Moreover, the magnetic susceptibility of the sample is significantly higher along the c-axis compared to the ab plane, indicating that the c-axis serves as the axis of easy magnetization. Figure 3(e) illustrates the magnetic hysteresis loop of the sample at various temperatures under out-of-plane fields. The M–H curve demonstrates a characteristic hysteresis loop typical of FM materials at a temperature of 2 K, featuring a coercive field of $H_C = 595$ Oe. As the temperature increases, H_C decreases due to enhanced thermal fluctuations, leading to a reduction in the area of the hysteresis loop. The field-dependent magnetization along the ab plane exhibits a nonlinear curve below 15 K and displays a small hysteresis at 2 K (Fig. 3(f)). With increasing temperature, the rise in thermal energy results in a significant decrease in the saturation magnetic fields of CTA-$MnBi_2Te_4$. The pronounced

discrepancy between ZFC and FC magnetization, along with the magnetic hysteresis loop, indicates an Ising-type exchange interaction[37] between adjacent Mn layers. Collectively, these features imply FM ordering with out-of-plane magnetic moment alignment in CTA-$MnBi_2Te_4$, where the IEC is effectively suppressed.

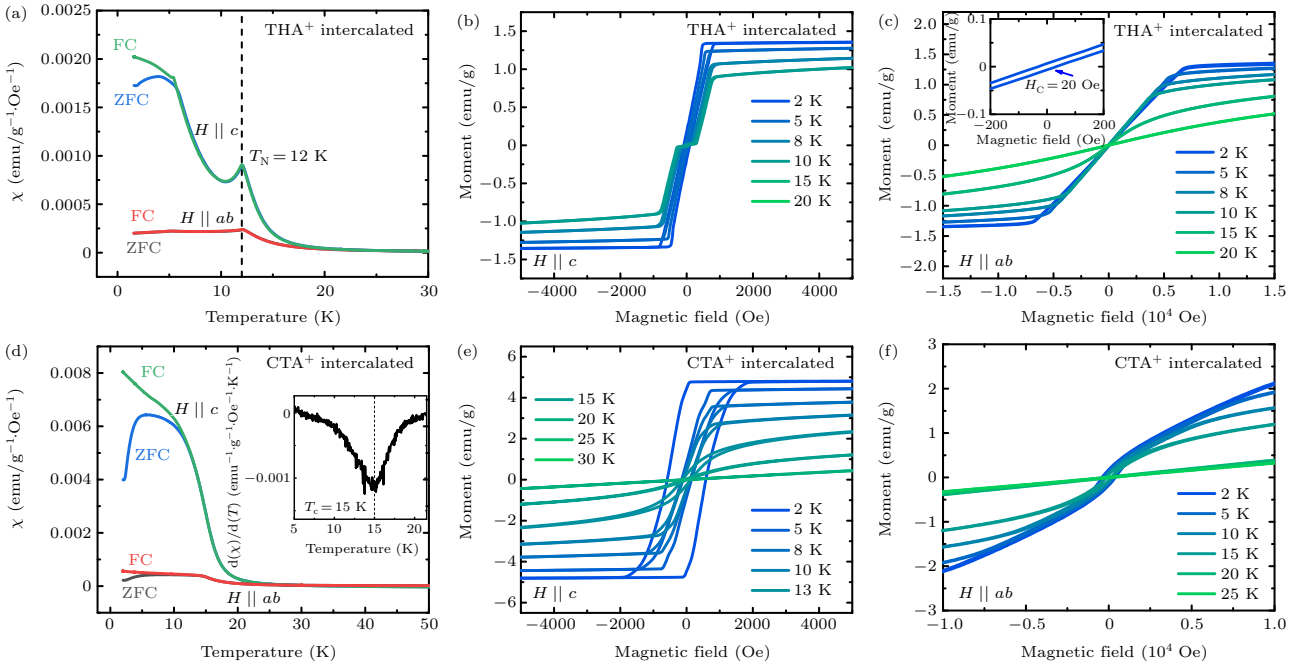


Fig. 3. (a) FC–ZFC curves of THA-$MnBi_2Te_4$ measured under an external magnetic field of 0.1 T. (b) Field-dependent magnetization curves of THA-$MnBi_2Te_4$ measured at various temperatures under an out-of-plane external magnetic field. (c) Field-dependent magnetization curves of THA-$MnBi_2Te_4$ measured at various temperatures under an in-plane external magnetic field. The inset shows field-dependent magnetization curves measured at 2 K. (d) FC–ZFC curves of CTA-$MnBi_2Te_4$ measured under an external magnetic field of 0.1 T. Temperature-dependent reciprocal susceptibility is shown in the inset. (e) Field-dependent magnetization curves of CTA-$MnBi_2Te_4$ measured at various temperatures under an out-of-plane external magnetic field. (f) Field-dependent magnetization curves of CTA-$MnBi_2Te_4$ measured at various temperatures under an in-plane external magnetic field.

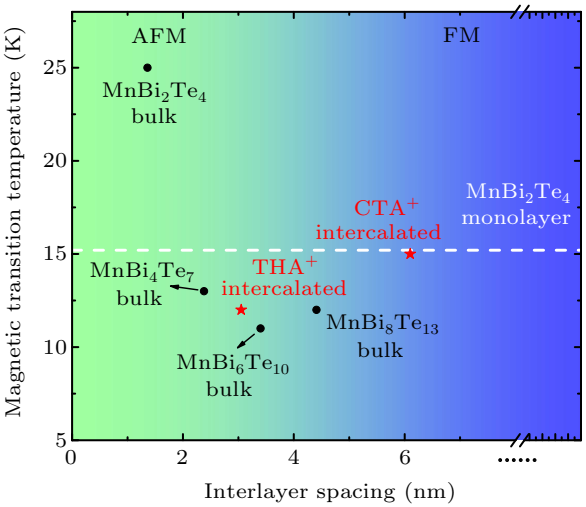


Fig. 4. Dependence of magnetic transition temperature on interlayer spacing of the $MnBi_2Te_4$-$(Bi_2Te_3)_m$ (m = 0, 1, 2, 3) family and organic-molecule-intercalated $MnBi_2Te_4$.

To elucidate the magnetic properties after the intercalation of organic cations in $MnBi_2Te_4$, we systematically summarize the magnetic transition temperatures of the $MnBi_2Te_4$-$(Bi_2Te_3)_m$ (m = 0, 1, 2, 3) family with varying interlayer spacings in Fig. 4. In $MnBi_2Te_4$, $MnBi_4Te_7$, and $MnBi_6Te_{10}$, these compounds exhibit an AFM state at T_N values of 25 K, 13 K, and 11 K, respectively.[29,41,50] According to previous studies,[50] the interlayer spacings of $MnBi_4Te_7$ and $MnBi_6Te_{10}$ are 23.8 Å and 33.9 Å, respectively. As illustrated in Fig. 2(c), the calculated interlayer spacing of THA-$MnBi_2Te_4$ is approximately 30.5 Å, with a T_N of 12 K. In the $MnBi_2Te_4$-$(Bi_2Te_3)_m$ (m = 0, 1, 2, 3) family, as the interlayer spacing increases to 44.1 Å, the m = 3 member ($MnBi_8Te_{13}$) transitions into the FM ground-state region, with T_C occurring at approximately 12 K.[29,37,50] When the interlayer spacing is fixed, substantial doping also enables effective modulation of the material's magnetic properties.[23] In $MnBi_4Te_7$, the energy difference between FM and AFM states is greatly reduced,[54] allowing Mn–Bi antisite defects to induce the coexistence of AFM and FM states. Therefore, we believe that modifying the interlayer spacing substantially affects the magnetic properties of $MnBi_2Te_4$ and that limited Mn–Bi antisite defects are unlikely to be the primary origin of the FM ordering observed below 2 K in THA-$MnBi_2Te_4$. When CTA^+ is intercalated into the vdW gap of $MnBi_2Te_4$, the interlayer spacing expands to 61.0 Å, and the material exhibits an FM critical temperature of 15 K. This value is consistent with that obtained for the $MnBi_2Te_4$ monolayer through RMCD measurements[51] in earlier research. We believe that electrochemical molecule intercalation provides an effective approach for modulating the magnetism of $MnBi_2Te_4$ and offers

a promising platform for exploring and realizing the QAHE and other topological quantum phenomena.

3. Conclusions and perspectives

In conclusion, owing to the limited investigations of the magnetic properties of monolayer $MnBi_2Te_4$, we present an effective method for electrochemically intercalating organic cations into the vdW gap of bulk $MnBi_2Te_4$. Upon the insertion of large-sized organic molecules, the interlayer spacing of $MnBi_2Te_4$ expands to 30.5 Å and 61.0 Å, respectively, thereby modulating its magnetic properties. The dual complex magnetic behavior observed in THA-$MnBi_2Te_4$ can be attributed to the coexistence of domains with both FM and AFM ordering between neighboring SLs. CTA-$MnBi_2Te_4$ exhibits an FM critical temperature (T_C) of 15 K and a coercive field (H_C) of 595 Oe. This T_C value is consistent with a previous study of $MnBi_2Te_4$ monolayers, confirming monolayer-like magnetism in our bulk-intercalated system. The changes in magnetic properties, including magnetic ground states, magnetic transition temperatures, and alterations in saturation magnetization and coercive field, are systematically investigated. Organic molecule intercalation not only provides a means to manipulate the magnetism of $MnBi_2Te_4$ but can also be readily extended to other vdW magnetic systems, offering a platform for the study of physical properties that cannot be accessed by other methods. The magnetic phases of $MnBi_2Te_4$ can be manipulated via different organic cations of various sizes, creating opportunities for applications in spintronics and nanoelectronics.

Appendix A: Methods

A1. Crystal growth

High-quality $MnBi_2Te_4$ single crystals are synthesized using the flux method. The raw materials, namely, MnTe and Bi_2Te_3, are mixed in a molar ratio of 1:5.85 in an alumina crucible, which is then sealed inside a quartz ampule. The ampule is placed in a furnace and heated to 950 °C over a period of one day. After maintaining it at 950 °C for 12 h, the ampule is cooled to 580 °C at a rate of 10 °C/h. Centrifugation is then carried out to remove the excess Bi_2Te_3 flux, yielding large crystals of $MnBi_2Te_4$.

A2. Electrochemical molecule intercalation

Intercalation is achieved through an electrochemical reaction using a simple lab-designed intercalation instrument. A graphite electrode serves as the anode, with the sample immobilized by a Cu clip electrode acting as the cathode. A silver/silver-chloride electrode is employed as the reference electrode. The potential difference between the reference electrode and the sample is monitored using an electrochemical workstation, which regulates the voltage applied between the graphite electrode and the sample to maintain a constant potential between the sample and the reference electrode. The organic molecule intercalation is carried out using a solution-based intercalation method, where 0.05 g of THAB or CTAB is dissolved in 20 ml of acetonitrile. The $MnBi_2Te_4$ single crystals are then immersed in the solution for a certain period at an applied electrochemical potential of −3.4 V. After the intercalation process, the samples are thoroughly washed with pure acetonitrile.

A3. Magnetic measurements

Magnetic measurements are performed using a vibrating sample magnetometer (VSM) option integrated with the physical property measurement system (PPMS, Quantum Design) with a minimum temperature of 1.8 K and a magnetic field of up to 14 T.

Acknowledgments

Project supported by the National Key Research and Development Program of China (Grant Nos. 2022YFA1402404 and 2023YFA1406304), the National Natural Science Foundation of China (Grant Nos. 92161201, T2221003, 12104221, 12104220, 12274208, 12025404, 12004174, 91961101, T2394473, 62274085, 12374043, and U2032208), the Natural Science Foundation of Jiangsu Province (Grant Nos. BK20230079, BK20243013, and BK20233001), and the Fundamental Research Funds for the Central Universities (Grant Nos. 020414380192 and 2024300432).

References

[1] Yu R, Zhang W, Zhang H J, Zhang S C, Dai X and Fang Z 2010 *Science* **329** 61
[2] Schaibley J R, Yu H, Clark G, Rivera P, Ross J S, Seyler K L, Yao W and Xu X 2016 *Nat. Rev. Mater.* **1** 16055
[3] Chang C Z, Zhang J, Feng X, Shen J, Zhang Z, Guo M, Li K, Ou Y, Wei P, Wang L L, Ji Z Q, Feng Y, Ji S, Chen X, Jia J, Dai X, Fang Z, Zhang S C, He K, Wang Y, Lu L, Ma X C and Xue Q K 2013 *Science* **340** 167
[4] Deng Y, Yu Y, Shi M Z, Guo Z, Xu Z, Wang J, Chen X H and Zhang Y 2020 *Science* **367** 895
[5] Li H, Ruan S and Zeng Y J 2019 *Adv. Mater.* **31** 1900065
[6] Wang Q H, Bedoya Pinto A, *et al.* 2022 *ACS Nano* **16** 6960
[7] Gong C, Li L, Li Z, Ji H, Stern A, Xia Y, Cao T, Bao W, Wang C, Wang Y, Qiu Z Q, Cava R J, Louie S G, Xia J and Zhang X 2017 *Nature* **546** 265
[8] Huang B, Clark G, Navarro Moratalla E, Klein D R, Cheng R, Seyler K L, Zhong D, Schmidgall E, McGuire M A, Cobden D H, Yao W, Xiao D, Jarillo Herrero P and Xu X 2017 *Nature* **546** 270
[9] Tan C, Lee J, Jung S G, Park T, Albarakati S, Partridge J, Field M R, McCulloch D G, Wang L and Lee C 2018 *Nat. Commun.* **9** 1554
[10] Du K Z, Wang X Z, Liu Y, Hu P, Utama M I B, Gan C K, Xiong Q and Kloc C 2016 *ACS Nano* **10** 1738
[11] Bonilla M, Kolekar S, Ma Y, Diaz H C, Kalappattil V, Das R, Eggers T, Gutierrez H R, Phan M H and Batzill M 2018 *Nat. Nanotechnol.* **13** 289
[12] O'Hara D J, Zhu T, Trout A H, Ahmed A S, Luo Y K, Lee C H, Brenner M R, Rajan S, Gupta J A, McComb D W and Kawakami R K 2018 *Nano Lett.* **18** 3125

[13] Otrokov M M, Klimovskikh I I, Bentmann H, *et al.* 2019 *Nature* **576** 416

[14] Gong Y, Guo J, Li J, Zhu K, Liao M, Liu X, Zhang Q, Gu L, Tang L, Feng X, Zhang D, Li W, Song C, Wang L, Yu P, Chen X, Wang Y, Yao H, Duan W, Xu Y, Zhang S C, Ma X, Xue Q K and He K 2019 *Chin. Phys. Lett.* **36** 076801

[15] Aliev Z S, Amiraslanov I R, Nasonova D I, Shevelkov A V, Abdullayev N A, Jahangirli Z A, Orujlu E N, Otrokov M M, Mamedov N T, Babanly M B and Chulkov E V 2019 *J. Alloys Compd.* **789** 443

[16] Zhang D, Shi M, Zhu T, Xing D, Zhang H and Wang J 2019 *Phys. Rev. Lett.* **122** 206401

[17] Li J, Li Y, Du S, Wang Z, Gu B L, Zhang S C, He K, Duan W and Xu Y 2019 *Sci. Adv.* **5** eaaw5685

[18] Liu C, Wang Y, Li H, Wu Y, Li Y, Li J, He K, Xu Y, Zhang J and Wang Y 2020 *Nat. Mater.* **19** 522

[19] Yan J Q, Zhang Q, Heitmann T, Huang Z, Chen K Y, Cheng J G, Wu W, Vaknin D, Sales B C and McQueeney R J 2019 *Phys. Rev. Mater.* **3** 064202

[20] Zeugner A, Nietschke F, Wolter A U B, Gaß S, Vidal R C, Peixoto T R F, Pohl D, Damm C, Lubk A, Hentrich R, Moser S K, Fornari C, Min C H, Schatz S, Kißner K, Ünzelmann M, Kaiser M, Scaravaggi F, Rellinghaus B, Nielsch K, Hess C, Büchner B, Reinert F, Bentmann H, Oeckler O, Doert T, Ruck M and Isaeva A 2019 *Chem. Mater.* **31** 2795

[21] Lee S H, Zhu Y, Wang Y, Miao L, Pillsbury T, Yi H, Kempinger S, Hu J, Heikes C A, Quarterman P, Ratcliff W, Borchers J A, Zhang H, Ke X, Graf D, Alem N, Chang C Z, Samarth N and Mao Z 2019 *Phys. Rev. Res.* **1** 012011

[22] Otrokov M M, Rusinov I P, Blanco Rey M, Hoffmann M, Vyazovskaya A Y, Eremeev S V, Ernst A, Echenique P M, Arnau A and Chulkov E V 2019 *Phys. Rev. Lett.* **122** 107202

[23] Chen B, Fei F, Zhang D, Zhang B, Liu W, Zhang S, Wang P, Wei B, Zhang Y, Zuo Z, Guo J, Liu Q, Wang Z, Wu X, Zong J, Xie X, Chen W, Sun Z, Wang S, Zhang Y, Zhang M, Wang X, Song F, Zhang H, Shen D and Wang B 2019 *Nat. Commun.* **10** 4469

[24] Hao Y J, Liu P, Feng Y, Ma X M, Schwier E F, Arita M, Kumar S, Hu C, Lu R e, Zeng M, Wang Y, Hao Z, Sun H Y, Zhang K, Mei J, Ni N, Wu L, Shimada K, Chen C, Liu Q and Liu C 2019 *Phys. Rev. X* **9** 041038

[25] Chen Y J, Xu L X, Li J H, Li Y W, Wang H Y, Zhang C F, Li H, Wu Y, Liang A J, Chen C, Jung S W, Cacho C, Mao Y H, Liu S, Wang M X, Guo Y F, Xu Y, Liu Z K, Yang L X and Chen Y L 2019 *Phys. Rev. X* **9** 041040

[26] Li H, Gao S Y, Duan S F, Xu Y F, Zhu K J, Tian S J, Gao J C, Fan W H, Rao Z C, Huang J R, Li J J, Yan D Y, Liu Z T, Liu W L, Huang Y B, Li Y L, Liu Y, Zhang G B, Zhang P, Kondo T, Shin S, Lei H C, Shi Y G, Zhang W T, Weng H M, Qian T and Ding H 2019 *Phys. Rev. X* **9** 041039

[27] Li B, Yan J Q, Pajerowski D M, Gordon E, Nedić A M, Sizyuk Y, Ke L, Orth P P, Vaknin D and McQueeney R J 2020 *Phys. Rev. Lett.* **124** 167204

[28] Li H, Liu S, Liu C, Zhang J, Xu Y, Yu R, Wu Y, Zhang Y and Fan S 2020 *Phys. Chem. Chem. Phys.* **22** 556

[29] Klimovskikh I I, Otrokov M M, Estyunin D, *et al.* 2020 *npj Quantum Mater.* **5** 54

[30] Li J, Yin Z C, Li Q X and Zhu J J 2025 *Chin. Phys. B* **34** 037501

[31] Zhong D, Seyler K L, Linpeng X, Cheng R, Sivadas N, Huang B, Schmidgall E, Taniguchi T, Watanabe K, McGuire M A, Yao W, Xiao D, Fu K M C and Xu X 2017 *Sci. Adv.* **3** e1603113

[32] Rhone T D, Chen W, Desai S, Torrisi S B, Larson D T, Yacoby A and Kaxiras E 2020 *Sci. Rep.* **10** 15795

[33] Hasan M Z and Kane C L 2010 *Rev. Mod. Phys.* **82** 3045

[34] Sun H, Xia B, Chen Z, Zhang Y, Liu P, Yao Q, Tang H, Zhao Y, Xu H and Liu Q 2019 *Phys. Rev. Lett.* **123** 096401

[35] Hu C, Gordon K N, Liu P, Liu J, Zhou X, Hao P, Narayan D, Emmanouilidou E, Sun H, Liu Y, Brawer H, Ramirez A P, Ding L, Cao H, Liu Q, Dessau D and Ni N 2020 *Nat. Commun.* **11** 97

[36] Tian S, Gao S, Nie S, Qian Y, Gong C, Fu Y, Li H, Fan W, Zhang P, Kondo T, Shin S, Adell J, Fedderwitz H, Ding H, Wang Z, Qian T and Lei H 2020 *Phys. Rev. B* **102** 035144

[37] Hu C, Ding L, Gordon K N, Ghosh B, Tien H J, Li H, Linn A G, Lien S W, Huang C Y, Mackey S, Liu J, Reddy P V S, Singh B, Agarwal A, Bansil A, Song M, Li D, Xu S Y, Lin H, Cao H, Chang T R, Dessau D and Ni N 2020 *Sci. Adv.* **6** eaba4275

[38] Deng H, Chen Z, Wołoś A, Konczykowski M, Sobczak K, Sitnicka J, Fedorchenko I V, Borysiuk J, Heider T, Pluciński Ł, Park K, Georgescu A B, Cano J and Krusin Elbaum L 2021 *Nat. Phys.* **17** 36

[39] Shi M Z, Lei B, Zhu C S, Ma D H, Cui J H, Sun Z L, Ying J J and Chen X H 2019 *Phys. Rev. B* **100** 155144

[40] Ding L, Hu C, Feng E, Jiang C, Kibalin I A, Gukasov A, Chi M, Ni N and Cao H 2021 *J. Phys. D: Appl. Phys.* **54** 174003

[41] Wu J, Liu F, Sasase M, Ienaga K, Obata Y, Yukawa R, Horiba K, Kumigashira H, Okuma S, Inoshita T and Hosono H 2019 *Sci. Adv.* **5** eaax9989

[42] Hu Y, Xu L, Shi M, Luo A, Peng S, Wang Z Y, Ying J J, Wu T, Liu Z K, Zhang C F, Chen Y L, Xu G, Chen X H and He J F 2020 *Phys. Rev. B* **101** 161113

[43] Xu L, Mao Y, Wang H, Li J, Chen Y, Xia Y, Li Y, Pei D, Zhang J, Zheng H, Huang K, Zhang C, Cui S, Liang A, Xia W, Su H, Jung S, Cacho C, Wang M, Li G, Xu Y, Guo Y, Yang L, Liu Z, Chen Y and Jiang M 2020 *Sci. Bull.* **65** 2086

[44] Jo N H, Wang L L, Slager R J, Yan J, Wu Y, Lee K, Schrunk B, Vishwanath A and Kaminski A 2020 *Phys. Rev. B* **102** 045130

[45] Rienks E D L, Wimmer S, Sánchez Barriga J, Caha O, Mandal P S, Růžička J, Ney A, Steiner H, Volobuev V V, Groiss H, Albu M, Kothleitner G, Michalička J, Khan S A, Minár J, Ebert H, Bauer G, Freyse F, Varykhalov A, Rader O and Springholz G 2019 *Nature* **576** 423

[46] Tan A, Labracherie V, Kunchur N, Wolter A U B, Cornejo J, Dufouleur J, Büchner B, Isaeva A and Giraud R 2020 *Phys. Rev. Lett.* **124** 197201

[47] Vidal R C, Bentmann H, Facio J I, Heider T, Kagerer P, Fornari C I, Peixoto T R F, Figgemeier T, Jung S, Cacho C, Büchner B, van den Brink J, Schneider C M, Plucinski L, Schwier E F, Shimada K, Richter M, Isaeva A and Reinert F 2021 *Phys. Rev. Lett.* **126** 176403

[48] Lu R, Sun H, Kumar S, Wang Y, Gu M, Zeng M, Hao Y J, Li J, Shao J, Ma X M, Hao Z, Zhang K, Mansuer W, Mei J, Zhao Y, Liu C, Deng K, Huang W, Shen B, Shimada K, Schwier E F, Liu C, Liu Q and Chen C 2021 *Phys. Rev. X* **11** 011039

[49] Zhong H, Bao C, Wang H, Li J, Yin Z, Xu Y, Duan W, Xia T L and Zhou S 2021 *Nano Lett.* **21** 6080

[50] Hu C, Qian T and Ni N 2023 *Natl. Sci. Rev.* **11**

[51] Yang S, Xu X, Zhu Y, Niu R, Xu C, Peng Y, Cheng X, Jia X, Huang Y, Xu X, Lu J and Ye Y 2021 *Phys. Rev. X* **11** 011003

[52] Lee D S, Kim T H, Park C H, Chung C Y, Lim Y S, Seo W S and Park H H 2013 *Cryst. Eng. Comm.* **15** 5532

[53] Li J, Wang C, Zhang Z, Gu B L, Duan W and Xu Y 2019 *Phys. Rev. B* **100** 121103

[54] Xie H, Wang D, Cai Z, Chen B, Guo J, Naveed M, Zhang S, Zhang M, Wang X, Fei F, Zhang H and Song F 2020 *Appl. Phys. Lett.* **116** 221902